THE JOURNAL OF BIOLOGICAL CHEMISTRY
Vol. 274, No. 6, Issue of February 5, pp. 3622–3631, 1999

Printed in U.S.A.

T Cell Recognition of Hapten

ANATOMY OF T CELL RECEPTOR BINDING OF A H-2K^d-ASSOCIATED PHOTOREACTIVE PEPTIDE DERIVATIVE*

(Received for publication, September 8, 1998, and in revised form, November 2, 1998)

Benedikt Kessler‡, Olivier Michielin§, Christopher L. Blanchard‡, Irina Apostolou¶, Christaiane Delarbre¶, Gabriel Gachelin¶, Claude Grégoire‖, Bernard Malissen‖, Jean-Charles Cerottini‡, Florian Wurm, Martin Karplus§, and Immanuel F. Luescher‡ ‡‡**

*From the ‡Ludwig Institute for Cancer Research, Lausanne Branch, University of Lausanne, 1066 Epalinges, Switzerland, the ¶Department of Immunology, INSERM U277, Pasteur Institute, 75015 Paris, France, ‖Centre d'Immunologie, INSERM/CNRS, 13288 Marseille-Luminy, France, §Institut Le Bel, Louis Pasteur University, 67404 Strasbourg, France, and **Centre for Biotechnology, Department of Chemistry EPFL, 1015 Lausanne, Switzerland*

To elucidate the structural basis of T cell recognition of hapten-modified antigenic peptides, we studied the interaction of the T1 T cell antigen receptor (TCR) with its ligand, the H-2K^d-bound *Plasmodium berghei* circumsporozoite peptide 252–260 (SYIPSAEKI) containing photoreactive 4-azidobenzoic acid (ABA) on *P. berghei* circumsporozoite Lys^{259}. The photoaffinity-labeled TCR residue(s) were mapped as Tyr^{48} and/or Tyr^{50} of complementary determining region 2β (CDR2β). Other TCR-ligand contacts were identified by mutational analysis. Molecular modeling, based on crystallographic coordinates of closely related TCR and major histocompatibility complex I molecules, indicated that ABA binds strongly and specifically in a cavity between CDR3α and CDR2β. We conclude that TCR expressing selective Vβ and CDR3α sequences form a binding domain between CDR3α and CDR2β that can accommodate nonpeptidic moieties conjugated at the C-terminal portion of peptides binding to major histocompatibility complex (MHC) encoded proteins.

CD8$^+$ cytotoxic T lymphocytes (CTL)[1] recognize by means of their T cell antigen receptor (TCR) antigenic peptides, usually 8–10 amino acids long, bound to major histocompatibility complex (MHC) class I molecules on target cells (1–4). However, CD8$^+$ (and CD4$^+$) T cells can also recognize antigenic peptides containing nonpeptidic moieties, such as carbohydrates or haptens, like trinitrophenyl, azobenzenearsonate, fluorescein, or phenylazides (5–15). Such T cells can be readily elicited and play a role in diseases, *e.g.* allergies, contact dermatitis, and eczema (16). The recognition of modified peptides is highly specific, and even small changes in the hapten or carbohydrate moiety can dramatically affect antigen recognition (13–18). This is reminiscent of immunoglobulins, which can be raised against and specifically bind such structures (19, 20). While x-ray crystallographic studies have revealed how antibodies bind haptens, little is known about how TCR do this. This is of particular interest, because TCR genes, unlike immunoglobulin genes, have no somatic mutations allowing affinity maturation. Moreover, TCR need to recognize hapten or carbohydrate moieties in the context of an MHC-peptide complex in a predefined orientation (21–25).

Available three-dimensional structures of TCR-ligand complexes revealed a consensus "diagonal" TCR-ligand orientation, in which the MHC-bound peptide runs diagonally between the CDR3 loops, extending from CDR1α to CDR1β (21, 23–25). In this orientation, the CDR3 loops can interact extensively with peptide side chains, which are mainly located in the center of MHC molecules, as well as with residues of the MHC α-helices. The α-helices of MHC class I molecules are elevated at the N-terminal portions; therefore, the approximately planar surface of the TCR ligand binding site can realize the best contact with the ligand in a diagonal orientation (21).

Hapten or carbohydrates conjugated with antigenic peptides are part of the epitope recognized by TCR (5, 8–15). TCR specific for hapten-modified antigenic peptides typically exhibit preferential usage of certain Vβ/Jα, and/or specific junctional sequences (13, 15, 18). We used as hapten photoreactive 4-azidobenzoic acid (ABA). This allowed assessment of TCR-ligand binding by TCR photoaffinity labeling and identification of the photoaffinity-labeled site(s), *i.e.* the contact(s) of the hapten with the TCR (13, 15).

We have previously generated and characterized two families of H-2K^d-restricted CTL clones, specific for two different photoreactive derivatives of the *Plasmodium berghei* circumsporozoite peptide PbCS-(252–260) (SYIPSAEKI) (13, 15). In one peptide derivative, ABA was conjugated with PbCS Lys^{259}, whereas P-255 was replaced by Lys(ABA) in the other. In addition, to prevent K^d-peptide derivative complex dissociation, PbCS Ser^{252} was replaced with iodo-4-azidosalicylic acid (IASA), which upon selective photoactivation permitted covalent attachment of the peptide derivative to K^d (26). The ABA, but not the IASA group, was part of the epitope recognized by these CTL. The two families of CTL clones were non-cross-reactive, and exhibited different TCR sequences (13, 15).

In this study, we describe the interaction of the TCR of the T1 CTL clones with its ligand, K^d-bound IASA-YIPSAEK-(ABA)I. Using mutational analysis, mapping of the photoaffinity-labeled site(s) and molecular modeling, we identified a specific binding mode, how the T1 TCR binds the ABA group. We propose that this binding principle has universal aspects.

* The costs of publication of this article were defrayed in part by the payment of page charges. This article must therefore be hereby marked "*advertisement*" in accordance with 18 U.S.C. Section 1734 solely to indicate this fact.

‡‡ To whom correspondence should be addressed: Ludwig Institute of Cancer Research, Chemin des Boversses 155, 1066 Epalinges, Switzerland. Tel.: 41 21 692 59 88; Fax: 41 21 653 44 74; E-mail: iluesche@eliot.unil.ch.

[1] The abbreviations used are: CTL, cytotoxic T lymphocyte(s); ABA, 4-azidobenzoic acid; CDR, complementary determining region; MHC, major histocompatibility complex; TCR, T cell antigen receptor(s); PbCS, *P. berghei* circumsporozoite; HPLC, high pressure liquid chromatography; PAGE, polyacrylamide gel electrophoresis; PCR, polymerase chain reaction; LZ, leucine zipper; IASA, iodo-4-azidosalicylic acid.

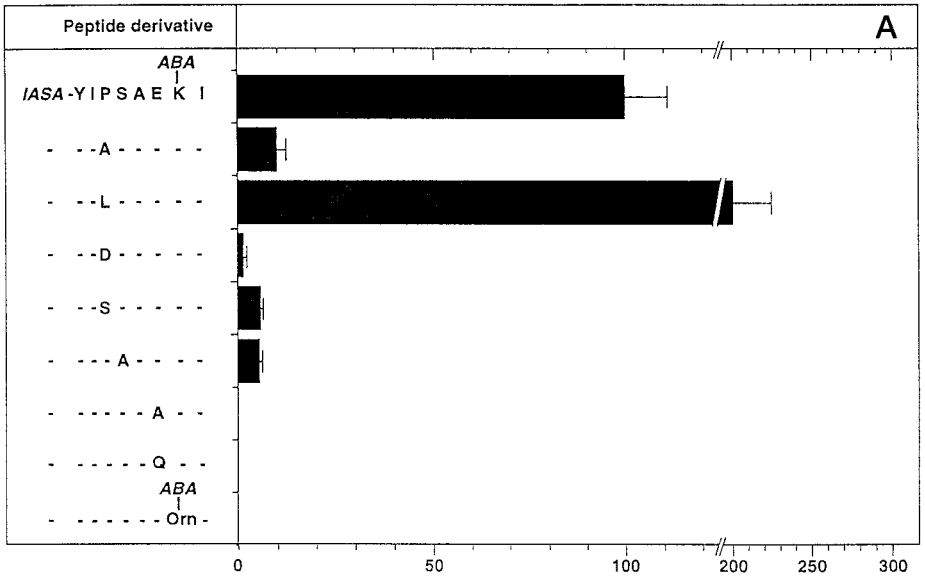

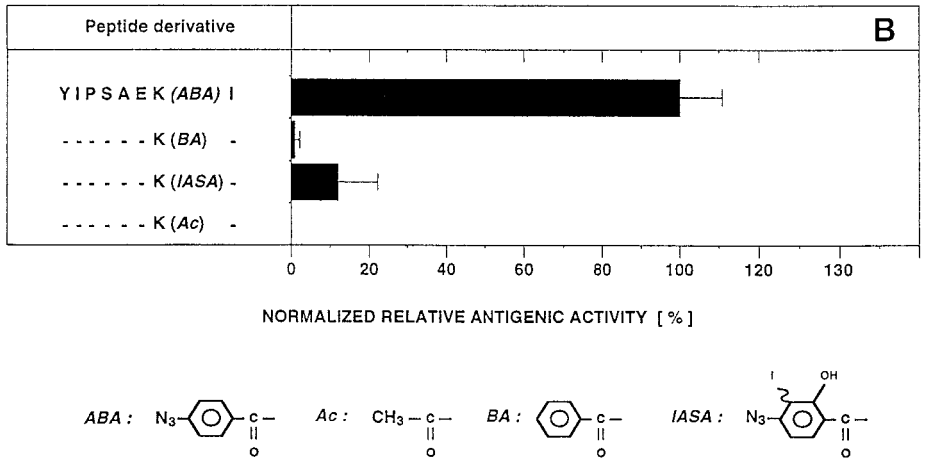

FIG. 1. **Effect of PbCS peptide derivative mutations on T1 TCR photoaffinity labeling and antigen recognition by T1 CTL.** *A*, the indicated radiolabeled peptide derivatives were photo-cross-linked to soluble K^d, and the resulting covalent K^d-peptide derivative complexes were used for TCR photoaffinity labeling on cloned T1 CTL. The labeling observed for K^d-^{125}IASA-YIPSAEK-(ABA)I was defined as 1, and labeling values for the ligand variants are expressed relative to this value. *B*, alternatively, the specific lysis of ^{51}Cr-labeled P815 cells was assessed in the presence of the indicated PbCS peptide derivatives. The antigenic activities are expressed relative to SYIPSAEK(ABA)I and normalized with the relative K^d competitor activities; thus, by definition the normalized relative antigenic activity of SYIPSAEK-(ABA)I was 1 (see "Experimental Procedures"). Each experiment was performed in triplicate and repeated at least once. The mean values and S.D. values were calculated from all experiments.

EXPERIMENTAL PROCEDURES

Peptide and Peptide Derivative Synthesis—Amino acids and other chemicals were obtained from Bachem Finechemicals AG (Bubendorf, Switzerland), Sigma Chemie (Buchs, Switzerland), and Neosystems (Strasbourg, France). Synthesis and characterization of peptide derivatives was performed as described previously (15, 17, 26). HPLC-purified peptide derivatives were reconstituted in PBS at 1 mM. The specific radioactivity of ^{125}I conjugates was approximately 2000 Ci/mmol.

Cellular Assays—For the cytolytic assay, ^{51}Cr-labeled P815 cells (5×10^3 cells/well) were incubated for 1 h at 37 °C in medium containing 10-fold dilutions of peptide derivatives, followed by UV irradiation at ≥350 nm. Cloned T1 CTL (1.5×10^4 cells/well) were added, and after 4 h of incubation at 37 °C, released ^{51}Cr was determined. The specific lysis was calculated as 100 × ((experimental − spontaneous release)/(total − spontaneous release)). The relative antigenic activities were calculated by dividing the concentration of IASA-YIPSAEK(ABA)I required for half-maximal lysis by that required for the variant peptide derivatives. These values were normalized by division with the corresponding relative K^d competitor activities (14, 15, 17).

K^d and TCR Photoaffinity Labeling—All photoaffinity labeling procedures were performed as described previously (15, 17). In brief, for TCR photoaffinity labeling, 10^7 cpm of K^d-^{125}IASA-YIPSAEK(ABA)I were incubated with 10^7 T1 CTL on ice for 3 h, followed by UV irradiation at 312 ± 40 nm. For peptide mapping, T1 CTL (4×10^7) were incubated likewise with K^d-SYIPSAEK(^{125}IASA)I (1 mCi) in 2 ml of medium containing β_2-microglobulin (2.5 μg/ml). After UV irradiation at ≥350 nm, cells were washed twice and lysed in phosphate-buffered saline (1×10^7 cells/ml) containing 0.7% Nonidet P-40, HEPES, phenylmethylsulfonyl fluoride, leupeptin, and iodoacetamide. The detergent-soluble fractions were subjected to immunoprecipitation with anti-TCR Cβ monoclonal antibody H57–597. The immunoprecipitates were analyzed by SDS-PAGE (10%, reducing conditions) and quantified using a PhosphorImager and the ImageQuant software (Molecular Dynamics, Inc., Sunnyvale, CA). S.D. values were calculated from 2–4 experiments.

Soluble T1 TCR and Mutants—T1 α and β cDNAs extending from the 5′ terminus up to, but not including, bases encoding the extracellular membrane-proximal cysteine residues were generated by reverse transcription on total T1 CTL RNA followed by polymerase chain reaction (PCR) amplification. The DNA fragments encoding a linker sequence and leucine zipper (LZ) components were generated by using oligonucleotides and PCR on templates pACID and pBASE (27). The T1 TCR-leucine zipper cDNAs were prepared by using recombinant PCR on these templates. The T1αLZ and T1βLZ cDNA containing basic and acidic LZ, respectively, were cloned into pCR-script (Stratagene) and subcloned into the *Eco*RI site of the mammalian expression vector pCI-neo (Promega). All PCR amplifications were performed using *Pfu* DNA polymerase (Stratagene), and both strands of cloned inserts were sequenced and found to be error-free. TCR mutants were generated using the QuickChange site-directed mutagenesis kit (Stratagene) following the suppliers instructions. 293T cells (ATCC) were transfected with pT1αLZ and pT1βLZ DNA (1:2 ratio) for transient expression of soluble αβT1 TCR following published procedures (28). After 2 days, supernatants were harvested, and T1 TCR concentrations were equalized. Preparation of T1 single chain Fv cDNA constructs and protein expression were performed as described previously (29).

Soluble K^d and Mutants of Soluble K^d—A full-length K^d cDNA cloned in pKC expression vector (promotor SV40, Hanahan) was double-di-

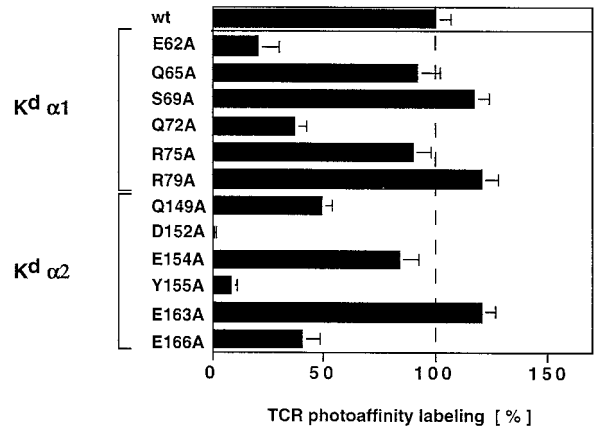

FIG. 2. **Effect of K^d mutations on T1 TCR photoaffinity labeling.** Soluble K^d molecules containing single alanine substitutions in the indicated position were photo-cross-linked with ^{125}IASA-YIPSAEK-(ABA)I, and their ability to photoaffinity-label T1 TCR was assessed as described for Fig. 2. Each experiment was performed 2–4 times.

gested with *Hin*dIII and *Xba*I in order to excise the sequences encoding the cytoplasmic and transmembrane domains up to nucleotide 966. The vector was religated using a *Hin*dIII–*Xba*I linker containing a stop codon, giving rise to translated C terminus RWKLA-stop. This K^d cDNA was cloned into the pcDNA3 expression vector (Invitrogen) under control of the cytomegalovirus promoter. Site-directed mutagenesis was performed using the Transformer^{TM} kit (CLONTECH) according to the manufacturer's instructions. Full-length cDNA coding for β2m was prepared and inserted in the same vector using the proper linkers (30).

Peptide Mapping—All procedures have been described previously (13, 15). Enzymes were obtained from Boehringer Mannheim (Rotkreuz, Switzerland) and used as recommended (31). In brief, photoaffinity-labeled T1 TCR was reduced, alkylated, and reconstituted in 500 μl of 100 mM Tris, pH 8.0 (for tryptic digests) or 100 mM phosphate buffer, pH 7.8 (for V8 digests) containing 10% acetonitrile. Aliquots of enzymes (10 μg) were added in 12-h intervals, and after 48 h of incubation at 37 °C, the digests were subjected to reverse phase HPLC on an analytical C-18 column (4 × 250 mm, 5-μm particle size, Vydac, Hisperia, CA). The column was eluted with a linear gradient of acetonitrile in 0.1% trifluoroacetic acid, rising within 1 h from 0 to 75%. Elution of radioactivity was monitored by γ-counting of 1-ml fractions. For destructive digestion the double-labeled V8 and Asp-N digest fragment was reconstituted in 300 μl of citrate buffer (50 mM, pH 5.5) containing 50 mM NaCl and Nonidet P-40 (0.01%) and incubated at 37 °C for 36 h with cathepsin C and carboxypeptidases P. Enzymes (5 μg) were added every 12 h. For biosynthetic labeling of T1 TCR with [^{3}H]tyrosine, CD8 α/β-transfected T1.4 T cell hybridomas (0.7 × 10^6) were incubated in tyrosine-deficient Dulbecco's modified Eagle's medium supplemented with fetal calf serum (5%) and 5 mCi of [^{3}H]tyrosine (NEN Life Science Products; specific activity of 142 Ci/mmol) at 37 °C for 20 h. The washed cells were photoaffinity-labeled with K^d-SYIPSAEK(^{125}IASA)I (specific radioactivity of 20 Ci/mmol). The M_r values of the labeled digest fragments were assessed by SDS-PAGE as described (32).

Molecular Modeling—A homology model of the T1 TCR and the K^d-SYIPSAEK(ABA)I complex was built using the MODELLER program (33) based on the crystal coordinates of TCR A6 (Vα2.3, Jα24; Vβ12.3, Jβ2.1)-HLA-A2-Tax peptide complex (21), TCR 2C (Vα3, Jα58; Vβ8.2, Jβ2.4) (22, 23), TCR 14.3 β-chain (Vβ8.2, Jβ2.1) (34), TCR 1934.4 Vα (Vα4.2) (35), and H2-K^b (3). The related sequences of corresponding chains were aligned using a dynamic programming method implemented in the MODELLER program (33). An all atom model of the complex was built using MODELLER by satisfaction of spatial restraints obtained from the alignment and parameters in the program. A distance restraint was introduced initially between the phenyl rings of ABA and β-Tyr^{48} and β-Tyr^{50}, respectively. Side chain orientations were optimized using a backbone-dependent rotamer library (36, 37). CDR1β and CDR2β loops were not subsequently refined, since their conformation was modeled from the TCR 2C, which has the same Vβ8.2 as TCR T1. For the other CDR loops, the conformations with the low energies were identified by simulated annealing with the rest of the structure fixed. From these, the final loop orientations were selected by using data from the mutation experiments. The resulting structure was refined with 500 steps of steepest descent energy minimization using the CHARMM (version 25) program (38) with the all-atom PARAM 22 parameter set (39). No significant violation of spatial restraints was found for β-Tyr^{48}, β-Tyr^{50}, and K(ABA) after optimization, indicating that the imposed distance restraint does not imply a distortion of the structure. Details concerning the modeling will be presented separately.[2]

RESULTS

Effect of PbCS Peptide Derivative Mutations on T1 TCR-Ligand Binding and Antigen Recognition by T1 CTL—To obtain information on PbCS(ABA) contacts with T1 TCR, several PbCS(ABA) variants were assessed by TCR photoaffinity labeling with soluble K^d-^{125}IASA-YIPSAEK(ABA)I complexes (Fig. 1*A*). The replacement of PbCS Pro^{255} by Ala, Asp, or Ser reduced T1 TCR labeling by 10-, 100-, and 17-fold, respectively, whereas replacement by Leu increased it 2-fold, suggesting that voluminous aliphatic residues in this position stabilize, and polar ones destabilize, T1 TCR-ligand binding. Alanine substitution of PbCS Ser^{256} impaired T1 TCR photoaffinity labeling by 95%. Substitution of PbCS Glu^{258} with alanine or glutamine obliterated detectable T1 TCR labeling, indicating that Glu^{258} forms a polar contact with T1 TCR. Shortening of PbCS Lys^{259} by one methylene group (YIPSAEOrn(ABA)I) also abolished T1 TCR labeling, indicating that the full spacer length was required.

To define the interaction of ABA with T1 TCR, PbCS(ABA) variants with modified ABA were examined. These nonphotoreactive compounds were assessed in a cytolytic assay as derivatives of SYIPSAEK(ABA)I (Fig. 1*B*). Cloned T1 CTL killed target cells sensitized with SYIPSAEK(benzoic acid)I approximately 100-fold less efficiently than those sensitized with SYIPSAEK(*ABA*)I. Replacement of the phenylazide by a methyl group (SYIPSAEK(Ac)I) obliterated detectable antigen recognition, while introduction of an iodine and hydroxy substituent in *ABA* (YIPSAEK(IASA)I) reduced the efficiency of antigen recognition by 8-fold. These results indicate that the phenylazide of the ABA moiety was essential for antigen recognition and that changes of substituents predictably affected the efficiency of recognition.

Effect of K^d Mutations on T1 TCR Photoaffinity Labeling—To identify K^d-TCR contacts, we prepared soluble K^d and 12 K^d mutants containing single alanine substitutions on the surface of the α1 or α2 helices (Fig. 2). After photo-cross-linking with radiolabeled ^{125}IASA-YIPSAEK(ABA)I, TCR-ligand binding was assessed by T1 TCR photoaffinity labeling, as described above. Six of the K^d mutations impaired T1 TCR-ligand binding by ≥50%. Two were on K$^d\alpha$1 (E62A and Q72A), and four were on K$^d\alpha$2 (Q149A, D152A, Y155A, and E166A). Some K^d mutations increased T1 TCR photoaffinity labeling by up to 20% (S69A, R79A, and E163A).

Effect of T1 TCR Mutations on T1 TCR Photoaffinity Labeling—To define ligand contact residues, soluble T1 TCR and 31 mutants were prepared and tested by T1 TCR photoaffinity labeling with soluble K^d-^{125}IASA-YIPSAEK(ABA)I (Fig. 3). Seven of these mutations reduced TCR photoaffinity labeling by ≥90%. Three of these were in CDR3 loops, three others were in CDR1, and one was in CDR2α. In addition, six other mutations reduced T1 TCR photoaffinity labeling by ≥50%. Four of these were in CDR2α, one was in CDR2β, and one was in CDR3α. Several mutations increased TCR photoaffinity labeling by up to 60% (*e.g.* αN27A, βY50F, and βT55A). Mutants labeled with an asterisk were T1 TCR Fv single chain constructs (29).

Localization of the Photoaffinity-labeled Site(s) on T1 TCR—To localize the photoaffinity-labeled site(s), T1 TCR was

[2] O. Michielin and M. Karplus, manuscript in preparation.

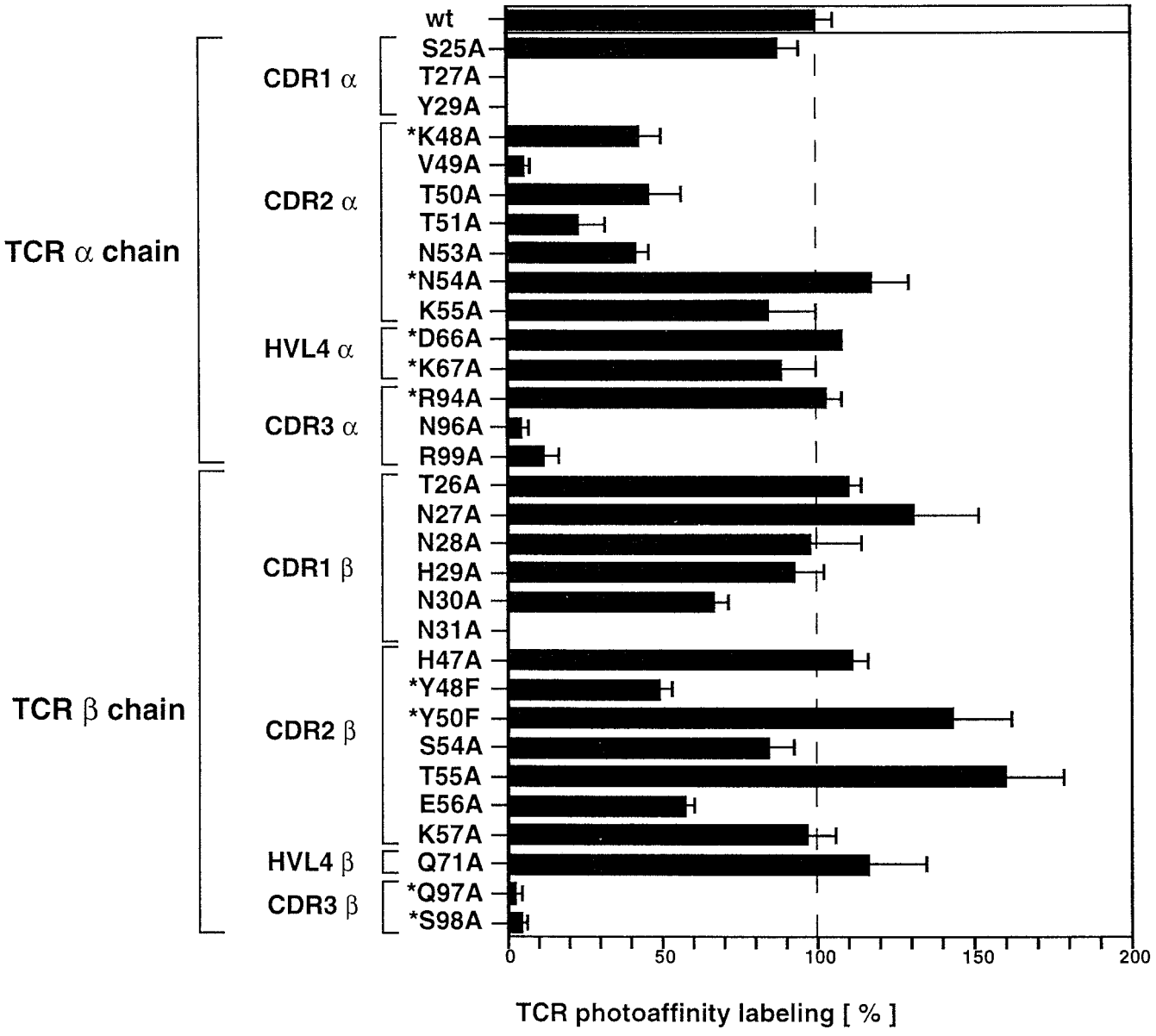

FIG. 3. **Effect of T1 TCR mutations on TCR photoaffinity labeling.** Soluble T1 TCR comprising the variable and constant domains of both chains and mutants containing single alanine substitutions in the indicated positions were incubated with soluble covalent K^d-^{125}IASA-YIPSAEK(ABA)I complexes at 0–4 °C for 30 min. After UV irradiation, TCR photoaffinity labeling was assessed as described for Fig. 2. The mutants labeled with an *asterisk* were single chain Fv T1 TCR constructs. The mean values and S.D. values were calculated from two experiments.

photoaffinity-labeled with SYIPSAEK(^{125}IASA)I, a derivative that was efficiently recognized by T1 CTL (Fig. 1*B*) and, being monovalent, precluded cross-linking with K^d. Since T1 TCR was photoaffinity-labeled exclusively at the β-chain (15), the photoaffinity-labeled TCR was directly subjected to peptide mapping. After extensive digestion with trypsin, the resulting digest fragments were separated by reverse phase HPLC. The major labeled digest fragment eluted from the C-18 column after 30 min and according to SDS-PAGE was homogenous and had an apparent M_r of approximately 3000 (Fig. 4, *lane 2*). When protease V8 was used instead of trypsin, a major labeled material eluted from the column after 32–33 min, which migrated on SDS-PAGE with an apparent M_r of approximately 8300 (Fig. 4, *lane 1*). The size of this fragment was bigger than any theoretical V8 fragment of the variable domain of the T1 TCR β-chain (Fig. 5*B*), suggesting that protease V8, even after extensive digestion, omitted a cleavage site. Since this enzyme primarily cleaves C-terminal to Glu and hence may fail to cleave after Asp (31), the labeled V8 digest product was digested with protease Asp-N. Essentially the same HPLC profile was observed; however, on SDS-PAGE this material migrated with an apparent M_r of approximately 2000 (Fig. 4, lane 3), indicating that V8 failed to cleave at an aspartic acid. This residue probably was β-Asp^{38}, because the big reduction in size (approximately 6300 Da) may correspond to the size of the segment 2–37, which contains the glycosylation site β-Asn^{24} (Fig. 5*B* and Ref. 34). Accordingly, the labeled V-8 digest fragment would be 2–56 (Fig. 5*B*).

To verify this, it was treated with CNBr, which cleaves at methionine residues. This resulted in the formation of a new labeled fragment, which eluted from the C18 column after 34–35 min and migrated on SDS-PAGE with an apparent M_r of approximately 2500 Da (Fig. 4, *lane 4*). Since the variable domain of the T1 TCR β-chain contains only one methionine, this confirmed that the labeled V-8 digest fragment consisted of residues 2–56 (Fig. 5*B*). The observed shift in M_r suggested that the labeled site(s) was located C-terminal to β-Met^{32}, *i.e.* in the segment 33–56. Moreover, the predicted labeled V8

digest fragment contains three arginine residues (Arg^{9}, Arg^{36}, and Arg^{44}). To assess their presence, it was partially digested (6 h) with Arg-C. As assessed by HPLC, this treatment produced earlier eluting radioactive materials, probably of mixed composition, as suggested by the broad range of elution (29–31 min). SDS-PAGE analysis of fractions 29–31 showed three new labeled species, migrating with apparent M_r of approximately 1800, 2600, and 7000, respectively, with the smaller ones eluting earlier from the HPLC column (Fig. 4, *lanes 5–7*). Upon extensive digestion with Arg-C, only the smallest fragment was observed (data not shown). These findings confirm that the labeled primary V8 digest fragment was residues 2–56 and suggest that the labeled site was contained in the segment 45–56.

To substantiate this, we tested whether the labeled digest fragment resulting after digestion with V8 and Asp-N contained an arginine, by extensively digesting it with Arg-C. This treatment resulted in a new labeled fragment that according to HPLC and SDS-PAGE was indistinguishable from the smallest fragment obtained after digestion of the labeled V8 digest fragment with Arg-C (Fig. 4, *lane 8*). By contrast, no change was observed when protease Lys-C was used (data not shown). Together, these findings demonstrate that the photoaffinity-labeled site(s) was contained in the uncharged sequence 45–56 (LIHYSYGAGSTE).

T1 TCR Photoaffinity Labeling Involved Tyrosine Residues—Because this sequence contains two tyrosines and ABA and IASA have low, but measurable affinity for tyrosine (14, 15), we examined whether the T1 TCR photoaffinity labeling involved tyrosine. To this end, T1 TCR was biosynthetically labeled with [^{3}H]tyrosine and photoaffinity-labeled with K^{d}-SYIPSAEK-(^{125}IASA)I. Following digestion with V8 and Asp-N, HPLC showed the same ^{125}I profile as observed previously and various ^{3}H-labeled materials (Fig. 6*A*). The ^{125}I-labeled material was extensively digested with cathepsin C and carboxypeptidase P. HPLC showed that the major ^{125}I-labeled material also contained ^{3}H (Fig. 6*B*). On SDS-PAGE, this material migrated at the gel front, *i.e.* had a M_r of less than 1000–1200, confirming extensive, probably complete degradation (data not shown). Tyrosine and monoiodotyrosine eluted from the HPLC column in fractions 6, 7, and 19, respectively, *i.e.* both earlier than the double-labeled digest fragment (Fig. 6*C*). These results indicate that the T1 TCR β-chain was photoaffinity-labeled at tyrosine residue(s) and demonstrate that this tyrosine modification was not a UV irradiation mediated trans-iodination.

Model of the T1 TCR-K^{d}-SYIPSAEK(ABA)I Complex—To evaluate our data in structural terms, we built a model of the T1 TCR-K^{d}-SYIPSAEK(ABA)I complex. Accurate homology modeling of the T1 TCR and K^{d} was made possible by the

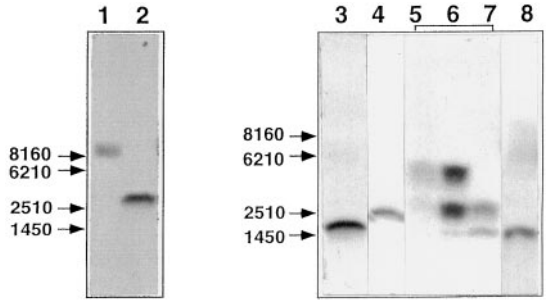

FIG. 4. **Localization of photoaffinity-labeled site(s) on T1 TCR β-chain.** T1 TCR was photoaffinity labeled with soluble K^{d}-SYIPSAEK(^{125}IASA)I and digested with different proteases. The resulting fragments were separated by C-18 reverse phase HPLC, and the ^{125}I-containing materials were analyzed by SDS-PAGE. *Lane 1*, V8 digest; *lane 2*, tryptic digest; *lane 3*, digest with V8 and Asp-N; *lane 4*, digest with V8 and CNBr cleavage; *lanes 5*, *6*, and *7*, HPLC fractions 31, 30, and 29, respectively, of V8 and Arg-C digest; *lane 8*, digest with V8, Asp-N, and Arg-C. Representative experiments are shown. Each experiment was repeated 1–5 times.

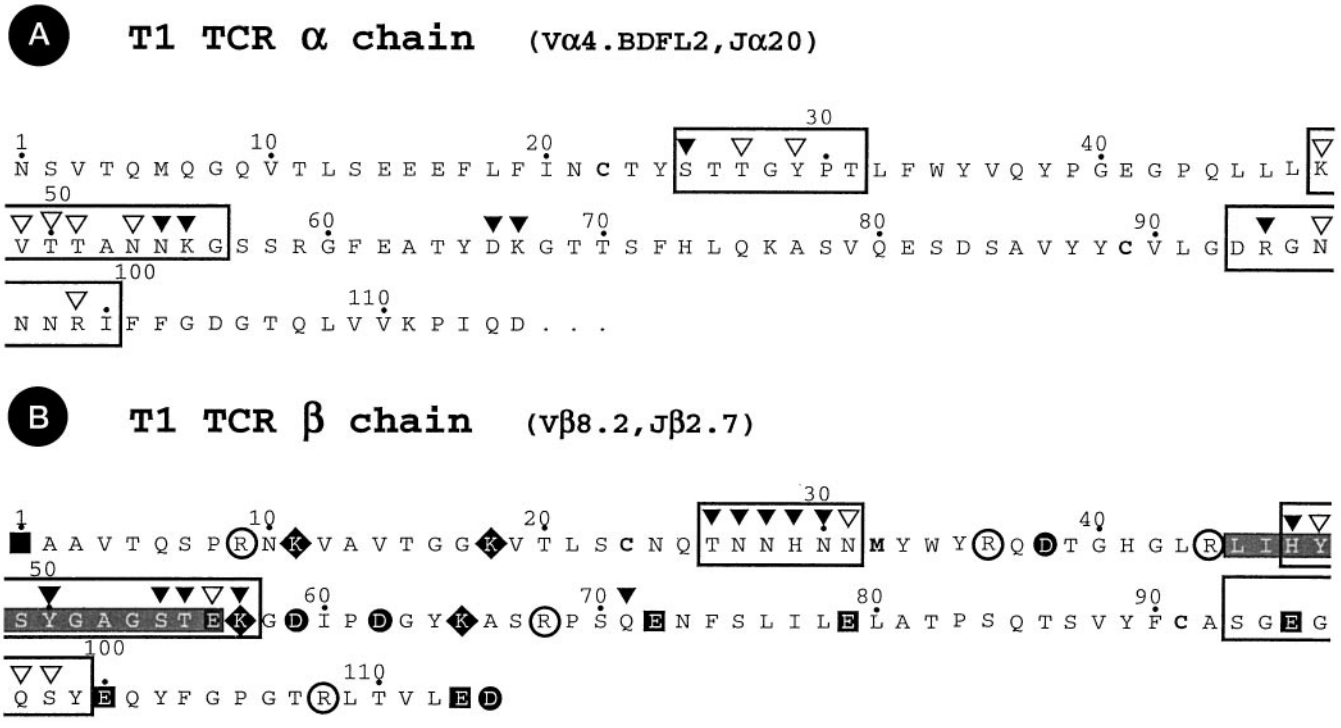

FIG. 5. **Amino acid sequence of T1 TCR α- and β-chain.** For the β-chain, which contains the labeled site(s), the cleavage sites for protease V8 (*E* and *D*) and for trypsin (*R* and *K*) are marked. Cysteines and methionines are printed in *boldface type*. The digest fragment 45–56 containing the photoaffinity-labeled site(s) is shown in *gray*. For both TCR chains, the CDR sequences are shown in *boxes*, and the residues subjected to mutational analysis are marked by *triangles*; *open triangles* indicate residues sensitive to mutation. The constant domains on both TCR chains start at position 112.

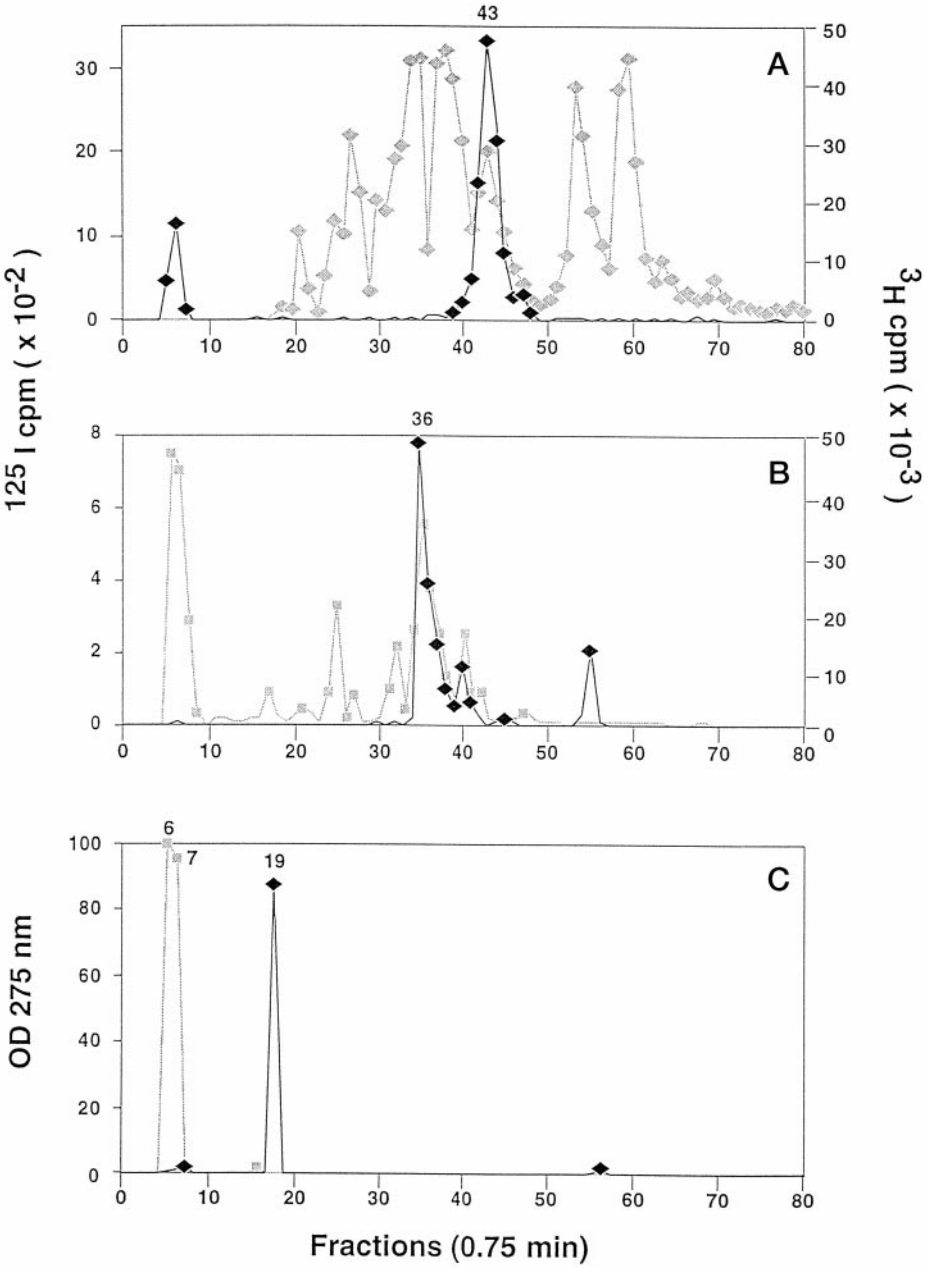

FIG. 6. **T1 TCR is photoaffinity-labeled at tyrosine residue(s).** *A*, soluble T1 TCR, biosynthetically labeled with [^{3}H]tyrosine, was photoaffinity-labeled with soluble K^d-SYIPSAEK(^{125}IASA)I. Following extensive digestion with protease V8 and Asp-N, the digest fragments were separated by C-18 reverse phase HPLC, and 0.75-ml fractions were counted for ^{125}I (*diamonds*) and ^{3}H (*squares*). *B*, the major ^{125}I-labeled material (fractions 42–44) was treated with cathepsin C and carboxypeptidase P, and the resulting fragments were analyzed likewise. The ^{125}I spill-over was subtracted from the ^{3}H cpm. *C*, as references, tyrosine (*squares*) and iodotyrosine (*diamonds*) were subjected to HPLC, and the OD was measured at 275 nm.

availability of crystal coordinates of closely related TCR and K^b (TCR 2C and TCR 14.3 express Vβ8.2 as TCR T1 and TCR 1934.4 expresses a Vα of the same subfamily). The Cα root mean square deviation between our model and (i) the Vβ of the 2C TCR was 0.35 Å, (ii) the Vα of the 1934.4 TCR was 1.68 Å, (iii) the variable domain of K^b was 0.53 Å, and (iv) the A6 TCR-HLA-A2-Tax peptide complexes was 1.83 Å (CDR3 included). The diagonal orientation of the T1 TCR relative to the K^d-PbCS(ABA) complex and the positioning of the CDR loops resulted in a pocket between CDR1β, CDR2β, and CDR3α. The bottom of the pocket is formed by α-Arg^{99} and β-Glu^{56}, one side by CDR3α residues Asn^{96} and Asn^{97} and the other side by CDR2β residues Tyr^{48}, Tyr^{50}, and Asn^{31} of CDR1β (Fig. 7). The Lys^{259}(ABA) side chain was orientated such that it inserts into this cavity between the side chains of β-Tyr^{48} and β-Tyr^{50}. The first two methylene groups of K259(ABA) have van der Waals contacts with K^d Trp^{73}, and the ABA carbonyl forms a hydrogen bond with its indol nitrogen. These interactions restrict the mobility of the K(ABA) side chain and keep it in a slanted orientation.

The phenyl rings of β-Tyr^{48}, β-Tyr^{50}, and ABA are nearly parallel and equally spaced at a distance of approximately 3.0 Å. This is in agreement with the finding that β-Tyr^{48} and/or β-Tyr^{50} were photoaffinity-labeled sites (Figs. 4 and 6). Five other TCR residues, α-Asn^{96}, α-Asn^{97}, α-Arg^{99}, β-Asn^{31}, and β-Glu^{95}, also interact with the ABA moiety. The δ-amide nitrogen (ND2) of α-Asn^{96} forms a hydrogen bond to the ABA carbonyl OF (see Table I for atom labels); the Cα of α-Asn^{97} makes a van der Waals contact with its CE2; OD1 of β-Asn^{31} makes a polar interaction of the C-H . . . *X* type with its CD1 and CE1 and OE1 of β-Glu^{95} with its NZ (Table I). There is also a weak hydrogen bond between the OH group of β-Tyr^{50} and ABA CE2 as well as a polar contact between the OH group of β-Tyr^{48} and N2 of ABA. Finally, there is a hydrogen bond between NH1 and NH2 of α-Arg^{99} and N3 of ABA. These interactions are consistent with the data from the mutational analysis (Figs. 1–3), although there was no quantitative evaluation of the free energies involved.

The K^d-bound peptide runs diagonally between the CDR3 loops, and its termini are located underneath the CDR1 loops

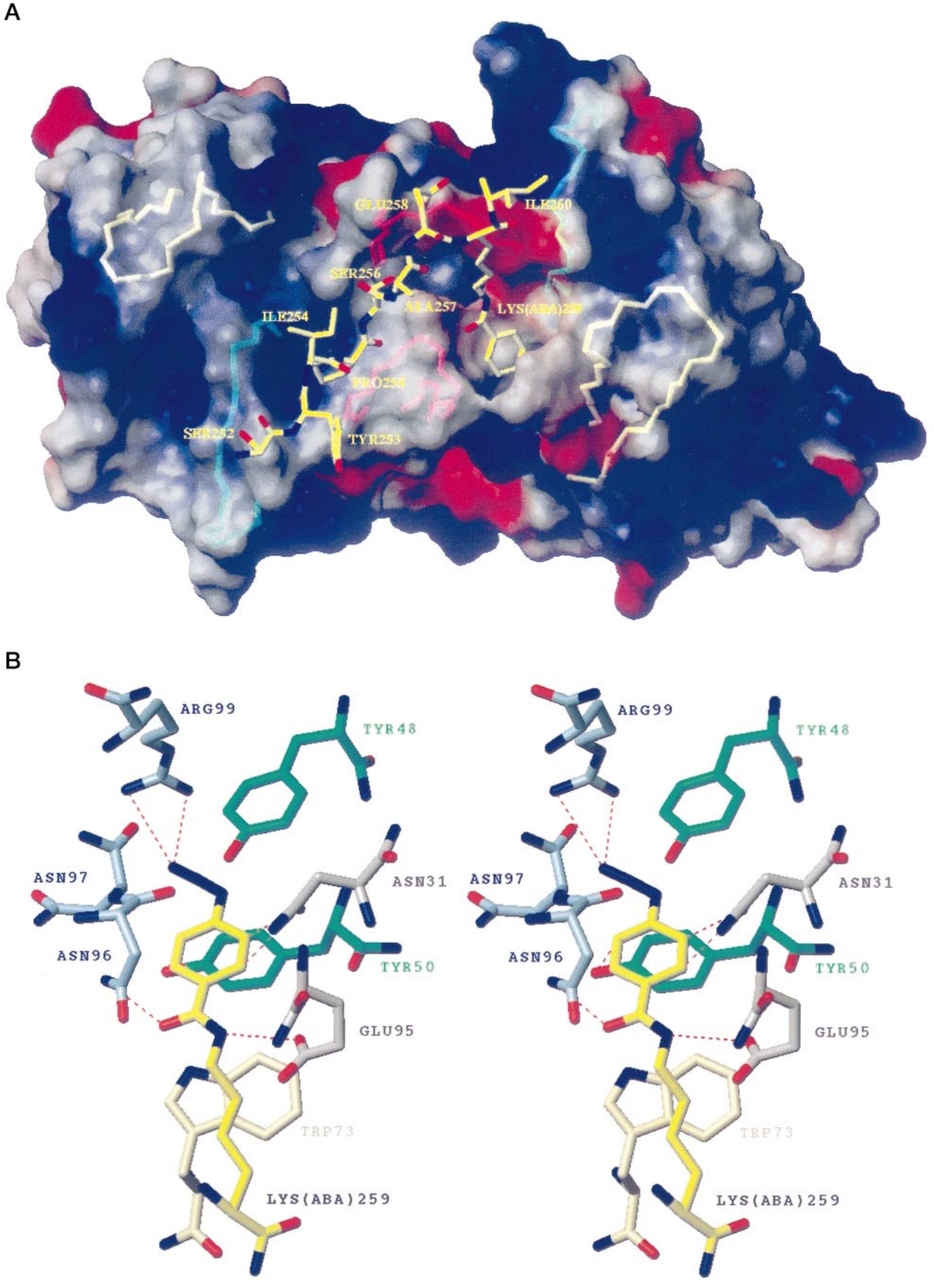

FIG. 7. **Molecular modeling of the T1 TCR-K^d-SYIPSAEK(ABA)I complex.** *A*, top view of the surface of the T1 TCR ligand binding site with bound SYIPSAEK(ABA)I in the bound state (α-chain on the *left* and β-chain on the *right*). Peptide residues are shown in *yellow*, surface-exposed acidic TCR residues are shown in *red*, and basic ones are shown in *blue*. The Cα backbones of the underlying CDR1 loops are shown in *light yellow*, those of the CDR2 loops are shown in *light green*, and those of the CDR3 loops are shown in *purple*. *B*, stereo view of K259(ABA) (*green*) and

TABLE I
T1 TCR-ligand contacts predicted by model

Contact No.	Location	TCR		Ligand		Distance[a]	Inhibition[b]	
							TCR	Ligand
						Å	%	
1	CDR1α	Thr^{26}	OG1[c]	K^d Glu^{58}	OE1	3.0*		
2	CDR1α	Thr^{27}	OG1[d]	K^d Glu^{58}	OE1	3.2*	99	
3	CDR1α	Tyr^{29}	OH[d]	K^d Glu^{62}	OE1	2.6*		99
4	CDR2α	Lys^{48}	NZ[d]	K^d Glu^{154}	OE1	2.8*	58	
5	CDR2α	Lys^{48}	NZ	K^d Tyr^{155}	OH	2.9*		92
6	CDR2α	Thr^{51}	OG1[c,d]	K^d Ala^{158}	CB	3.3	78	
7	CDR2α	Asn^{53}	ND2[c]	K^d Glu^{166}	OE2	3.5*	58	60
8	CDR3α	Arg^{94}	O	PbCS Pro^{255}	CG	3.1		90
9	CDR3α	Gly^{95}	CA	PbCS Pro^{255}	CB	3.2		
10	CDR3α	Asn^{96}	ND2	ABA[e]	OF	2.8*	96	
11	CDR3α	Asn^{96}	N	PbCS Pro^{255}	O	3.3*	96	
12	CDR3α	Asn^{97}	CA	ABA	CE2	3.1		
13	CDR3α	Arg^{99}	NH1	ABA	N3	3.2*	88	100
14	CDR3α	Arg^{99}	NH2	ABA	N3	3.4*		
15	βN terminus	Glu^{1}	OE2	K^d Gln^{149}	NE2	2.9*		50
16	CDR1β	Asn^{31}	OD1	ABA	CE1	2.7*	99	
17	CDR1β	Asn^{31}	OD1	ABA	CD1	3.1*	99	
18	CDR2β	Tyr^{48}	OH	ABA	N2	3.6	51	100
19	CDR2β	Tyr^{50}	OH	ABA	CE2	3.2*	60	
20	CDR2β	Tyr^{50}	OH	K^d Gln^{72}	OE1	2.9*	60	66
21	CDR3β	Glu^{95}	OE1	ABA	NZ	3.1*		
22	CDR3β	Gln^{97}	NE2	PbCS Glu^{258}	OE1	3.1*	98	99
23	CDR3β	Gln^{97}	N	PbCS Glu^{258}	OE1	3.0	98	99
24	CDR3β	Gln^{97}	NE2	K^d Asp^{152}	OD1	2.7*	98	100
25	CDR3β	Gln^{97}	OE1	K^d Asp^{152}	N	2.9*	98	100
26	CDR3β	Ser^{98}	OG	K^d Tyr^{155}	OH	2.9*	96	92
27	CDR3β	Tyr^{99}	OH	K^d Tyr^{159}	OH	2.7*		

[a] Asterisks denote hydrogen bonds; no asterisk signifies van der Waals or polar contacts.
[b] Inhibition of T1 TCR photoaffinity labeling upon mutation.
[c] As observed for A6 TCR (21).
[d] As observed for 2C TCR (23).
[e] Nonstandard atom designation used for ABA:

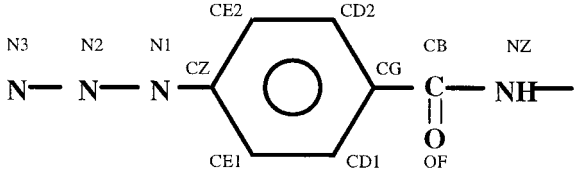

(Fig. 7*A*). According to the model, residues K^d Glu^{58}, Glu^{62}, Gln^{72}, Gln^{149}, Asp^{152}, Glu^{154}, Ala^{158}, Tyr^{155}, Tyr^{159}, and Glu^{166} form hydrogen bonds with T1 TCR (Table I). Alanine substitution of the underlined residues significantly reduced T1 TCR photoaffinity labeling (Fig. 2). The predicted contacts with K^d Glu^{58} and Ala^{158} are in accordance with TCR mutational analysis (Fig. 3). TCR-MHC contacts 1, 6, and 7 (Table I) were also observed in the A6 TCR-HLA-A2-Tax complex (21), and the contacts 2–4 and 6 were observed in the 2C TCR-K^b-dEV8 complex (23). According to the model, the PbCS residues Pro^{255}, Ser^{256}, Glu^{258}, and Lys^{259}(ABA) interact with T1 TCR (Table I). Indeed, mutation of these residues, especially of Glu^{258} and Lys^{259}(ABA), substantially impaired T1 TCR photoaffinity labeling or antigen recognition by T1 CTL (Fig. 1). For Pro^{255}, the model shows that the upper part of the nonpolar proline ring makes a van der Waals contact with the methylene group of α-Gly^{95} and a hydrogen bond with O of α-Arg^{94}, which is consistent with the observation that replacement of Pro^{255} with Ala, Ser, Asn, or Asp decreased T1 TCR photoaffinity labeling (Fig. 1). For PbCS Ser^{256}, the model predicts a hydrogen bond between its OH group and OD1 of αN96, and for PbCS Glu^{258} contacts with β-Gln^{97} and K^d Lys^{146}. Alanine substitution of β-Gln^{97} dramatically reduced T1 TCR photoaffinity labeling (Fig. 3) and of K^d Lys^{146} peptide binding to K^d (data not shown), since this residue also interacts with the C-terminal carboxyl group of the peptide (3, 4).

DISCUSSION

The present study uses peptide mapping, mutational analysis, and molecular modeling to describe in structural terms how TCR can avidly and specifically bind a hapten-modified peptide in the context of a MHC class I molecule. The hapten, photoreactive ABA, conjugated at the penultimate residue of the PbCS peptide SYIPSAEKI, constituted an essential part of the epitope recognized by T1 CTL (Figs. 1 and 2). The fact that peptide mapping allowed localization of the photoaffinity-labeled site(s) on T1 TCR (Figs. 4 and 6) indicates that this labeling was site-specific. In view of the high chemical reactivity of the radicals produced by UV irradiation (14, 15) of phenylazides and the flexible nature of the lysine side chain, this implies that the ABA group associated with the T1 TCR in a well defined orientation. If this were not so, heterogeneous photo-cross-linking would occur to preclude reproducible and resolved peptide mapping (40).

contacting T1 TCR residues. CDR3α residues are shown in *light blue*, CDR2β residues are shown in *dark yellow*, CDR1β and CDR3β residues are shown in *white*, and K^d Trp^{73} is shown in *light yellow*. The *dotted lines* indicate hydrogen bonds. The *images* were produced with the MOLMOL program (42).

To better understand in structural terms the interaction of the photoreactive ligand side chain with the T1 TCR, we modeled the T1 TCR-K^d-SIPSAEK(ABA)I complex. While available crystal coordinates of related TCR and MHC class I molecules permitted homology modeling of most of the system with good accuracy, the main problems concerned the docking the TCR to the ligand and the positioning of certain CDR loops. The docking was based on the diagonal orientation observed for all TCR-ligand complexes whose three-dimensional structures have been elucidated (21, 23–25). This orientation involves conserved TCR-MHC class I contacts, mainly between TCR Vα and residues of the MHC α1 and α2 helices (21, 23, 24). Our model is in accordance with these contacts. Moreover, we made use of the interaction of ABA with β-Tyr^{48} and β-Tyr^{50}, as indicated by the observations that (i) the T1 TCR was photoaffinity-labeled at tyrosines of the CDR2β segment 45–56 (LIHYSYGAGSTE) (Figs. 4 and 6); (ii) TCR of the same specificity, which expressed β-Tyr^{48}, but not β-Tyr^{50}, were photoaffinity-labeled also at the α-chain (15); (iii) ABA and IASA have low affinities for Tyr and Trp (14); and (iv) TCR-ligand binding, as assessed by inhibition of T1 TCR photoaffinity labeling by the soluble Fv T1 TCR, correlated with TCR photoaffinity labeling, except for the mutants βY48F and βY50F.[3]

According to the model, ABA inserts between the side chains of β-Tyr^{48} and β-Tyr^{50}, which are part of a pocket between CDR2β and CDR3α (Fig. 7). This position is energetically favorable and provides extensive π-π interactions and hydrogen bond formation (Table I). The ABA group was placed initially with a constraining potential between these tyrosine side chains, but it moved very little in subsequent energy minimization. The model shows that nine contacts, involving seven different TCR residues, further stabilize the interaction of the Lys(ABA) side chain with T1 TCR (Table I). This is a consequence of a specific three-dimensional arrangement of CDR3α, CDR3β, CDR2β, and CDR1β residues around the Lys(ABA) side chain. Mutation of these TCR residues, as well as modification of the Lys(ABA) side chain significantly affected T1 TCR photoaffinity labeling and antigen recognition by T1 CTL (Figs. 1 and 3). Similarly, TCR specific for peptides conjugated with benzoarsonate or fluorescein also utilize residues from different CDR loops for hapten binding (6, 41).

While our model is in good agreement with most of the mutational data, it failed to account for the effects of three TCR mutations (αV49A, αT50A, and βE56A) (Fig. 3 and Table I). Possible explanations include the following. (i) Certain mutations may result in conformational changes of CDR loops (*e.g.* the side chain of α-Val^{49} is in the center of CDR2α and forms various contacts with the peptide backbone; therefore, the αV49A mutation probably affects the CDR2α loop conformation). (ii) Some mutations may affect intramolecular amino acid interactions, resulting in reorientation of side chains engaged in TCR-ligand contacts (*e.g.* β-Glu^{56} forms a hydrogen bond with α-Arg^{99}, which interacts with N3 of *ABA*; thus, the βE56A mutation may be explained by reorientation of the α-Arg^{99} side chain). (iii) Water was not included in the model, which may account for some of these divergences.

Interestingly, the majority of CTL clones obtained from mice immunized with *IASA*-YIPSAEK(ABA)I expressed Vβ1- and JαTA28-encoded TCR, which were photoaffinity-labeled at both chains (15). For one of them, the photoaffinity labeled sites were identified as JαTA28-encoded tryptophan 97 and a residue of the Vβ1 segment 46–51, which contains β-Tyr^{48}, but not β-Tyr^{50} (15). It thus appears that for these TCR, the ABA group was inserted between α-Trp^{97} (CDR3α) and β-Trp^{48} (CDR2β), rather than two Vβ-encoded tyrosines.

Although the interaction of ABA with T1 TCR constituted an important part of T1 TCR-ligand binding, free peptide derivative, even at high concentration (10 μM), was unable to photoaffinity-label T1 TCR.[3] However, it has been reported that in other systems hapten in polymeric form or hapten-conjugated peptides at high concentrations can directly bind to TCR, *i.e.* that some hapten-reactive T cells may have promiscuous MHC restriction (7, 10). This is reminiscent of antibodies that can strongly bind small organic molecules. As shown by x-ray crystallography, such antibodies utilize residues from different CDR loops (19, 20). Comparison of the three-dimensional structures of the complexes of fluorescein with a monoclonal anti-fluorescein antibody and a fluorescein-specific TCR showed that both molecules use very similar principles in binding hapten (19, 41). Although TCR specific for hapten-modified peptides are unlikely to achieve the high affinities by which antibodies can bind hapten, they may reach higher affinities than TCR specific for conventional peptides, since cells expressing such high affinity TCR are prone to be eliminated by negative selection.

The present study suggests that TCR are able to bind specifically hapten-conjugated peptides by selection of particular Vβ and CDR3α sequences. From the data and the model, Vβ-encoded residues of CDR1 and mainly CDR2 play a key role in binding the Lys(ABA) side chain; however, residues of CDR3β and CDR3α spatially and electronically complement these interactions to an integral and sophisticated binding mode (Fig. 7, Table I). We suggest that this binding principle has universal aspects, *i.e.* that TCR expressing selected Vβ and CDR3α sequences are able to specifically bind haptens conjugated at the penultimate residue of MHC binding peptides by means of a pocket between CDR2β and CDR3α. As far as is known, and presumably for reasons of chemical reactivity, most "hapten-reactive" TCR recognize antigenic peptides containing a hapten-conjugated lysine (5, 11, 12). The long and flexible nature of the lysine side chain enables haptens to bind in this cavity, in the framework of the canonical diagonal orientation of TCR-ligand binding.

We and others have previously observed that CTL can also be readily elicited and specifically recognize haptens conjugated in position 4 or 5 of the peptide (11, 13). In a previous study, we mapped the photoaffinity labeled site(s) for a TCR specific for IASA-YIK(ABA)SAEKI (13). The labeled site(s) was located in the Vα-encoded C-strand segment 33–39, and computer modeling suggested that the Lys(ABA) side chain inserted into a pocket between the two CDR3 loops (13). Three-dimensional structure analysis showed that TCR indeed have a cavity between the CDR3 loops and that it can accommodate side chains of MHC-bound peptides (21, 22, 24).

These results provide significant insights into the structural basis of T cell recognition of hapten-conjugated MHC binding peptides. TCR expressing selected Vβ and CDR3α sequences can form cavities between CDR loops that can accommodate peptide-conjugated haptens in a highly specific manner (Fig. 7 and Refs. 13 and 15). The structural variability required for this is based mainly on junctional diversity, but V-encoded TCR sequences, in some cases even framework residues, play a role as well. This is consistent with the observation that hapten-reactive T cells typically express different TCR sequences than those recognizing the parental epitope (13–15).

Acknowledgments—We thank Drs. E. Bernasconi and M. Jordan for excellent technical assistance; Drs. D. Kuznetsov and V. Jongeneel for computational work; Drs. R. Stote, D. York, and X. Lopez for aid in determining force field parameters for the ABA group; and J. Muller and K. Rey for preparing the manuscript.

[3] B. Kessler, O. Michielin, C. L. Blanchard, I. Apostolou, C. Delarbre, G. Gachelin, C. Grégoire, B. Malissen, J.-C. Cerottini, F. Wurm, M. Karplus, and I. F. Luescher, unpublished data.

REFERENCES

1. Matis, L. A. (1990) *Annu. Rev. Immunol.* **8**, 65–82
2. Bjorkman, P. J. (1997) *Cell* **89**, 167–170
3. Fremont, D. H., Stura, E. A., Matsumura, M., Peterson, P. A., and Wilson, I. A. (1995) *Proc. Natl. Acad. Sci. U. S. A.* **92**, 2479–2483
4. Madden, D. R., Garboczi, D. N., and Wiley, D. C. (1993) *Cell* **75**, 693–708
5. Nalefski, E. A., and Rao, A. (1993) *J. Immunol.* **150**, 3806–3816
6. Nalefski, E. A., Kasibhatla, S., and Rao, A. (1992) *J. Exp. Med.* **175**, 1553- 1563
7. Siliciano, R. F., Hemesath, T. J., Pratt, J. C., Dintzis, R. Z., Dintzis, H. M., Acuto, O., Shin, H. S., and Reinherz, E. L. (1986) *Cell* **47**, 161–171
8. Harding, C. V., Kihlberg, J., Elofsson, M., Magnusson, G., and Unanue, E. R. (1993) *J. Immunol.* **151,** 2419–1425
9. Jensen, T., Hansen, P., Galli-Stampino, L., Mouritsen, S., Frische, K., Meinjohanns, E., Meldal, M., and Werdelin, O. (1997) *J. Immunol.* **158**, 3769–3778
10. Kohler, J., Hartmann, U., Grimm, R., Pflugfelder, U., and Weltzien, H. U. (1997) *J. Immunol.* **158**, 591–597
11. Martin, S., von Bonin, A., Fessler, C., Pflugfelder, U., and Weltzien, H. U. (1993) *J. Immunol.* **151**, 678–687
12. Martin, S., Ortmann, B., Pflugfelder, U., Birsner, U., and Wetzien, H. U. (1992) *J. Immunol.* **149**, 2569–2575
13. Anjuère, F., Kuznetsov, D., Romero, P., Cerottini, J.-C., Jongeneel, V., and Luescher, I. F. (1997) *J. Biol. Chem.* **272**, 8505–8514
14. Romero, P., Casanova, J.-L., Cerottini, J.-C., Maryanski, J. L., and Luescher, I. F. (1993a) *J. Exp. Med.* **177**, 1245–1256
15. Luescher, I. F., Anjuère, F., Peitsch, M. C., Jongeneel, V., Cerottini, J.-C., and Romero, P. (1995) *Immunity* **3**, 51–63
16. Hess, D. A., and Rieder, M. J. (1997) *Ann. Pharmacother.* **31**, 1378–1387
17. Kessler, B. M., Bassanini, P., Cerottini, J.-C., and Luescher, I. F. (1997) *J. Exp. Med.* **185**, 629–640
18. Preckel, T., Gimm, R., Martin, S., and Weltzien, H. U. (1997) *J. Exp. Med.* **185**, 1803–1813
19. Bedzyk, W. D., Herron, J. N., Edmundson, A. B., and Voss, E. W., Jr. (1990) *J. Biol. Chem* **265**, 133–138
20. Strong, R. K., Campbell, R., Rose, D. R., Petsko, G. A., Sharon, J., and Margolies, M. N. (1991) *Biochemistry* **30**, 3739–3748
21. Garboczi, D. N., Ghosh, P., Utz, U., Fan, Q. R., Biddison, W. E., and Wiley, D. C. (1996) *Nature* **384**, 134–141
22. Garcia, K. C., Degano, M., Stanfield, R. L., Brunmark, A., Jackson, M. R., Peterson, P. A., Teyton, L., and Wilson, L. A. (1996) *Science* **274**, 209–219
23. Garcia, K. C., Degano, M., Pease, L. R., Huang, M., Peterson, P. A., Teyton, L., and Wilson, I. A. (1998) *Science* **279**, 1166–1172
24. Ding, Y. H., Smith, K. J., Garboczi, D. N., Utz, U., Biddison, W. E., and Wiley, D. C. (1998) *Immunity* **8**, 403–411
25. Teng, M. K., Smolyar, A., Tse, A. G. D., Liu, J. H., Liu, J., Hussey, R. E., Nathenson, S. G., Chang, H. C., Reinherz, E. L., and Wang, J. H. (1998) *Curr. Biol.* **8**, 409–410
26. Luescher, I. F., Cerottini, J.-C., and Romero, P. (1994) *J. Biol. Chem.* **269**, 5574–5582
27. Chang, H. C., Bao, Z. Z., Yao, Y., Tse, A. G. D., Goyarts, E. C., Madsen, M., Kawasaki, E., Brauer, P. P., Sacchettini, J. C., Nathenson, S. G., and Reinherz, E. L. (1994) *Proc. Natl. Acad. Sci. U. S. A.* **91**, 11408–11412
28. Jordan, M., Schallhorn, A., and Wurm, F. M. (1996) *Nucleic Acids Res.* **24**, 596–601
29. Grégoire, C., Lin, S. Y., Mazza, G., Rebai, N., Luescher, I. F., and Malissen, B. (1996) *Proc. Natl. Acad. Sci. U. S. A.* **93**, 7184–7189
30. Godeau, F., Casanova, J.-L., Fairchild, K. D., Saucier, C., Delarbre, C., Gachelin, G., and Kourilsky, P. (1991) *Res. Immunol.* **142**, 409–416
31. Keesey, J. (1987) *Biochemicals for Protein Research*, pp. 87–108, Boehringer Mannheim, Indianapolis, IN
32. Schragger, A., and von Jagow, G. (1987) *Anal. Biochem.* **166**, 368–379
33. Sali, A., and Blundell, T. L. (1993) *J. Mol. Biol.* **234**, 779–815
34. Bentley, G. A., Boulot, G., Karjalainen, K., and Mariuzza, R. A. (1995) *Science* **267**, 1984–1987
35. Fields, B. A., Ober, B., Malchiodi, E. L., Lebedeva, M. I., Braden, B. C., Ysern, X., Kim, J. K., Shao, X., Ward, E. S., and Mariuzza, R. A. (1995) *Science* **270**, 1821–1824
36. Dunbrack R. L., and Karplus, M. (1994) *Nat. Struct. Biol.* **1,** 334–340
37. Bower, J. M., Cohen, F. E., and Dunbrack, R. L. (1997) *J. Mol. Biol.* **267,** 1268–1282
38. Brooks, B. R., Bruccoleri, R. E., Olasfon, B. D., States, D. J., Swaminathan, S., and Karplus, M. (1983) *J. Comp. Chem.* **4,** 187–217
39. MacKerell, A. D., Jr., Bashford, D., Bellott, M., Dunbrack, R. L., Jr., and Karplus, M. (1998) *J. Phys. Chem.* **102,** 3586–3616
40. Luescher, I. F., Crimmins, D. L., Schwarz, B. D., and Unanue, E. R. (1990) *J. Biol. Chem* **265**, 11177–11184
41. Ganju, R. K., Smiley, S. T., Bajorath, J., Novotny, J., and Reinherz, E. L. (1992) *Proc. Natl. Acad. Sci. U. S. A.* **89**, 11552–11556
42. Koradi, R., Billeter, M., and Wüthrich, K. (1996) *J. Mol. Graphics* **14,** 51–55